PCCP

PAPER

View Article Online
View Journal

Cite this: DOI: 10.1039/c6cp01147k

Theory of diffusion-influenced reactions in complex geometries†

Marta Galanti,[abcde] Duccio Fanelli,[ac] Sergey D. Traytak[f] and Francesco Piazza*[a]

Received 19th February 2016,
Accepted 17th May 2016

DOI: 10.1039/c6cp01147k

www.rsc.org/pccp

Chemical transformations involving the diffusion of reactants and subsequent chemical fixation steps are generally termed "diffusion-influenced reactions" (DIR). Virtually all biochemical processes in living media can be counted among them, together with those occurring in an ever-growing number of emerging nano-technologies. The role of the environment's geometry (obstacles, compartmentalization) and distributed reactivity (competitive reactants, traps) is key in modulating the rate constants of DIRs, and is therefore a prime design parameter. Yet, it is a formidable challenge to build a comprehensive theory that is able to describe the environment's "reactive geometry". Here we show that such a theory can be built by unfolding this many-body problem through addition theorems for special functions. Our method is powerful and general and allows one to study a given DIR reaction occurring in arbitrary "reactive landscapes", made of multiple spherical boundaries of given size and reactivity. Importantly, ready-to-use analytical formulas can be derived easily in most cases.

Diffusion-influenced reactions (DIRs) are ubiquitous in many contexts in physics, chemistry and biology[1,2] and they keep on sparking intense theoretical and computational activity in many fields.[3–10] Modern examples of emerging nanotechnologies that rely on the controlled alteration of diffusion and reaction pathways in DIRs include different sorts of chemical and bio-chemical catalysis involving complex nano-reactors,[11,12] nanopore-based sequencing engines,[13] morphology control and surface functionalization of inorganic-based delivery vehicles for controlled intracellular drug release.[14,15]

However, while the mathematical foundation for the description of such problems has been laid nearly a century ago,[16] many present-day problems of utmost importance at both the fundamental and applied levels are still challenging. Notably, arduous difficulties arise in the quantification of the important role played by the environment's geometry (obstacles, compartmentalization)[17] and distributed reactivity (patterns of competitive reaction targets or traps) in coupling transport and reaction pathways in many natural and artificial (bio)chemical reactions.[1,18,19]

A formidable challenge in modeling environment-related effects on chemical reactions is represented by the intrinsic many-body nature of the problem. This is brought about essentially by two basic features, common to virtually all realistic situations, namely the (i) finite density of reactants and other inert species (in biology also referred to as macromolecular crowding[20,21]) and (ii) confining geometry of natural or artificial reaction domains in 3D space. In general, the presence of multiple reactive and non-reactive particles/boundaries cannot be neglected in the study of (bio)-chemical reactions occurring in real milieux, where the geometrical compactness of the environment may have profound effects, such as first-passage times that are non-trivially influenced by the starting point.[22] Relevant complex media include the cell cytoplasm,[8,23–25] porous or other artificial confining media,[22,26–31] which can be considered as offering important tunable features for technological applications.[11,13,15]

In this paper, we take a major step forward by solving the general problem of computing the steady-state reaction rate for an irreversible bulk diffusion-influenced chemical reaction between a mobile ligand and an explicit arbitrary, static 3D configuration of spherical reactive boundaries of arbitrary sizes and intrinsic reactivities.

To set the stage for the forthcoming discussion, let us first consider the simple problem of two molecules A and B of sizes R and a, respectively, diffusing in solution. Upon encountering, the two species can form a complex, which catalyzes the transformation of species B into some product P with rate constant k,

$$\mathrm{A} + \mathrm{B} \xrightarrow{k} \mathrm{A} + \mathrm{P} \qquad (1)$$

[a] Università degli Studi di Firenze, Dipartimento di Fisica e Astronomia and CSDC, via G. Sansone 1, IT-50019 Sesto Fiorentino, Firenze, Italia. E-mail: Francesco.Piazza@gmail.com
[b] Dipartimento di Sistemi e Informatica, Università di Firenze, Via S. Marta 3, 50139 Florence, Italy
[c] INFN, Sezione di Firenze, Italy
[d] Université d'Orléans, Château de la Source, 45100, Orléans, France
[e] Centre de Biophysique Moléculaire, CNRS-UPR4301, Rue C. Sadron, 45071, Orléans, France
[f] Semenov Institute of Chemical Physics RAS, 4 Kosygina St., 117977 Moscow, Russia

† Electronic supplementary information (ESI) available. See DOI: 10.1039/c6cp01147k

Under the hypotheses that (i) A molecules diffuse much more slowly than B molecules, (ii) both species are highly diluted and (iii) the bulk concentration of A molecules ρ_A is much smaller than the bulk concentration of B molecules ρ_B,[2,32] the rate constant k can be computed by solving the following stationary two-body boundary problem[1]

$$\nabla^2 u = 0 \text{ with } u|_{\partial\Omega} = 0, \quad \lim_{r\to\infty} u = 1 \tag{2}$$

where $\partial\Omega$ is a spherical sink of radius $\sigma = R + a$ (the encounter distance) and $u(r) = \rho(r)/\rho_B$ is the stationary normalized concentration of B molecules around the sink. The rate constant is simply the total flux into the sink, *i.e.*

$$k = D\int_{\partial\Omega_0} \left.\frac{\partial u}{\partial r}\right|_{r=\sigma} \mathrm{d}S \tag{3}$$

where $D = D_A + D_B$ is the relative diffusion constant. The solution to the boundary-value problem (2) is $u(r) = 1 - \sigma/r$, which yields the so-called Smoluchowski rate constant for an isolated spherical sink, namely $k_S = 4\pi D\sigma$. These simple ideas, originally developed to describe coagulation in colloidal systems,[16,33] together with the related subsequent major advances by Debye[34] and Collins & Kimball[35] represent the basic building block of many modern theoretical approaches in chemical and soft-matter[36,37] kinetics.

In many realistic situations in chemical and biochemical kinetics, a single ligand (B) molecule has to diffuse among many competing reactive particles A. In addition, it might be forced to find its target within a specific confining geometry, which in principle can be modeled through a collection of reflecting boundaries. Such settings define a genuine many-body problem, as the overall flux of ligands is shaped by the mutual screening among all the different reactive boundaries (the reactive environment), known as diffusive interaction.[38–40] In the following, we show how these kinds of problems can be formulated and solved in a rather general form.

Let us imagine a reaction of kind (1) to be catalyzed at $N + 1$ spherical boundaries $\partial\Omega_\alpha$ of radius (encounter distance) $\sigma_\alpha = R_\alpha + a$, $\alpha = 0, 1, \ldots, N$ arranged in space at positions X_α. With reference to the Smoluchowski problem, this means that we are explicitly relaxing the assumption of vanishing density of the reactive centers A. In the most general setting, each sphere can be endowed with an intrinsic reaction rate constant k_α*, which specifies the conversion rate from the encounter complex to the product at its surface. Then, the stationary density of B molecules is the solution of the following boundary value problem

$$\nabla^2 u = 0 \tag{4a}$$

$$\left(\sigma_\alpha \frac{\partial u}{\partial r_\alpha} - h_\alpha u\right)\Big|_{\partial\Omega_\alpha} = 0 \quad \alpha = 0, 1, \ldots, N \tag{4b}$$

$$\lim_{r\to\infty} u = 1 \tag{4c}$$

where $h_\alpha = k_\alpha^*/k_{S_\alpha}$ with $k_{S_\alpha} = 4\pi D\sigma_\alpha$. The boundary conditions (BCs) (4b) are called radiative or Robin boundary conditions. The limits $h_\alpha \to \infty$ and $h_\alpha = 0$ correspond to perfectly absorbing (sink) and reflecting (obstacle) boundaries, respectively, while the values $0 < h_\alpha < \infty$ correspond to finite surface reactivity.[35]

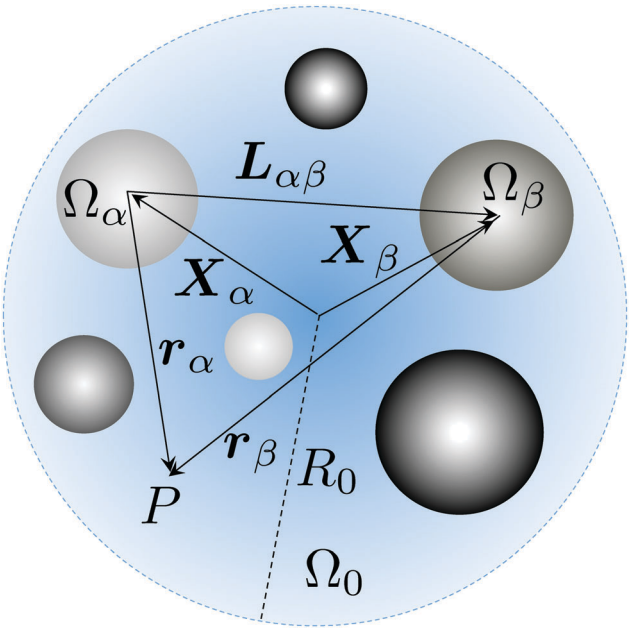

Fig. 1 Illustration of a multi-sink configuration. A number of active spheres of radius σ_α are located at positions X_α within the spherical domain Ω_0 of radius R_0. In this paper we solve the problem in the unbounded domain ($R_0 \to \infty$, see ESI† for the general solution). A given point P is identified by as many position vectors as there are spherical boundaries.

The boundary problem (4a)–(4c) provides a rigorous mathematical description of a wide assortment of physical situations, ranging from one or many sinks screened by the neighboring competing reactive boundaries to hindered diffusion to a sink located among a collection of static reflecting obstacles placed at given positions in space. As a worked example in molecular biology, a parallel paper by the same authors describes how our algorithm can be employed to investigate an important problem in molecular biology, *i.e.* the role of protein conformation in the binding process with a small ligand.[41]

In order to solve the problem, it is expedient to consider as many sets of spherical coordinate systems as there are boundaries, $r_\alpha \equiv (r_\alpha, \theta_\alpha, \phi_\alpha)$ (see Fig. 1). Hence, for any point $P \in \Omega$, the solution can be written formally as an expansion in a series of irregular solid harmonics, namely

$$u = 1 + \sum_{\alpha=0}^{N} u_\alpha^-(r_\alpha), \quad u_\alpha^- = \sum_{\ell=0}^{\infty}\sum_{m=-\ell}^{\ell} \frac{B_{m\ell}^\alpha}{r_\alpha^{\ell+1}} Y_{m\ell}(r_\alpha) \tag{5}$$

where r_α are the coordinates of P in the local frame centered on the α-sphere and $Y_{m\ell}(r_\alpha, \theta_\alpha, \phi_\alpha)$ are spherical harmonics.‡

The coefficients $B_{m\ell}^\alpha$ should be determined by imposing the BCs (4b). In order to do so, we use the known translation addition theorems for solid spherical harmonics[42,43] to express the solution (5) in all the $N + 1$ different coordinate systems

‡ Here we use the definition $Y_{m\ell}(\theta,\phi) = P_\ell^m(\cos\theta)e^{im\phi}$, where $P_\ell^m(\cos\theta)$ are associated Legendre polynomials.[42]

centered at each sphere. The result is the following infinite-dimensional system of linear equations

$$B^{\alpha}_{gq} - \frac{q-h_\alpha}{h_\alpha+q+1}\left(\delta_{g0}\delta_{q0} + \sum_{\ell=0}^{\infty}\sum_{m=-\ell}^{\ell}\sum_{\substack{\beta=0\\ \beta\neq\alpha}}^{N} B^{\beta}_{m\ell} W^{\alpha\beta gq}_{m\ell}\right) = 0 \quad (6)$$

for $\alpha = 0, 1, \ldots, N$, $q = 1, 2, \ldots, \infty$ and $g = -q, -q+1, \ldots, q-1, q$ (see ESI† for a detailed derivation and the explicit expression of the matrix elements $W^{\alpha\beta gq}_{m\ell}$). To solve the problem one simply needs to truncate the sum on ℓ in eqn (6), by including a finite number of multipoles so as to attain the desired accuracy for the overall rate constant. In analogy to eqn (3), and taking into account definition (5), the rate constant corresponding to a given subset of reactive boundaries $\mathscr{S}$ can be computed as

$$k = D\sum_{\alpha\in\mathscr{S}}\int_{\partial\Omega_\alpha}\left.\frac{\partial u}{\partial r}\right|_{r=\sigma_\alpha} \mathrm{d}S = -\sum_{\alpha\in\mathscr{S}} k_{\mathrm{S}_\alpha} B^{\alpha}_{00} \quad (7)$$

The theoretical framework that culminates in formula (7) serves as an extremely powerful tool to investigate how specific geometries of obstacles and/or competitive reactive boundaries modulate the rate constant of a given diffusion-influenced reaction.

A clear and instructive illustration of our general approach can be outlined by focussing on the simplest model of diffusion-influenced reaction, namely diffusion of a ligand to a perfect sink. Even if our method could be employed to examine far more complex reactive geometries, realized by assembling a large number of spherical boundaries of arbitrary sizes and reactivities, for the sake of clarity, we shall focus here on the case of a sink of radius σ surrounded by N identical spheres of radius $\sigma_1 = \lambda\sigma$ arranged randomly at a fixed distance d. This problem has been tackled recently for $\lambda = 1$ and $N \leq 4$ through a numerical finite-element (FE) method in ref. 40. This study provided clear-cut hints of the subtle effects brought about by the environment's geometry, but also highlighted the impossibility of brute-force numerical approaches to assess the impact of more crowded and sophisticated reactive environments.

In Fig. 2 we compare the FE numerical results with the exact solution for $N = 2$. It appears clear that the screening effect is harder to capture *via* a FE scheme in the case of reflecting obstacles than in the presence of competitive sinks. However, our exact approach allows one to dig much further into this problem and investigate analytically the screening effect of configurations comprising a large number of spheres. For example, one can expand the system (6) in powers of $\varepsilon \equiv \sigma/d$ to derive simple analytical estimates of the rate constant to the sink (see ESI† for detailed calculations). In the case of reflecting obstacles, one gets

$$\frac{k}{k_{\mathrm{S}}} = 1 - \left(\frac{\lambda^3 N}{2}\right)\varepsilon^4 - \left(\frac{2\lambda^5 N}{3}\right)\varepsilon^6 + \ldots \quad (8)$$

which is independent of the screening configuration and linear in N, as suggested in ref. 40. However, we find that this only holds up to the sixth order in ε – it can be seen from the expansion that the configuration enters explicitly successive

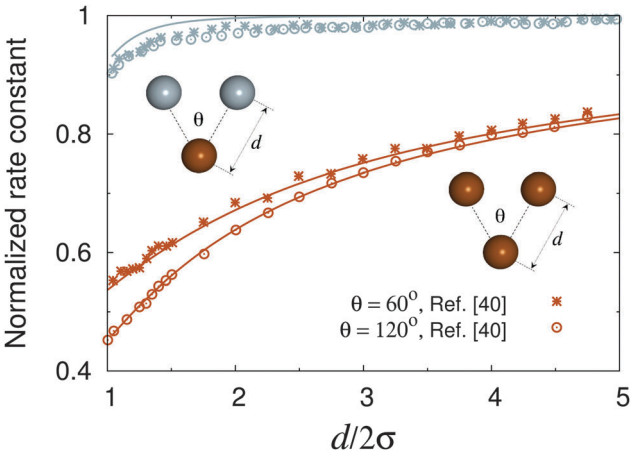

Fig. 2 The approximate finite-element calculations compared with the exact results. Total flux into a sink of radius σ normalized to $k_{\mathrm{S}} = 4\pi D\sigma$ (flux into an isolated sink) in the presence of two spherical screening boundaries of the same radius placed at a fixed distance d from the sink and forming an angle θ. Light blue and dark orange denote reflecting and absorbing particles, respectively. Symbols are numerical results of finite-element calculations from ref. 40. Solid lines are the corresponding exact results, obtained by solving eqn (6) with a relative accuracy of 10^{-4} with the same choices of parameters as indicated by the symbol legends (orange: absorbing, light blue: reflecting).

powers of ε (see ESI†). On the other hand, a similar procedure in the case of N screening sinks yields

$$\frac{k}{k_{\mathrm{S}}} = 1 - \lambda N\varepsilon + \left[\lambda N + \lambda^2\sum_{\substack{\alpha,\beta=1\\ \beta\neq\alpha}}^{N}\frac{1}{\Gamma_{\alpha\beta}}\right]\varepsilon^2 - \left[\lambda^2 N^2 + \lambda^2\sum_{\substack{\alpha,\beta=1\\ \beta\neq\alpha}}^{N}\frac{1}{\Gamma_{\alpha\beta}} + \lambda^3\sum_{\substack{\alpha,\beta,\delta=1\\ \beta,\delta\neq\alpha}}^{N}\frac{1}{\Gamma_{\alpha\beta}\Gamma_{\alpha\delta}}\right]\varepsilon^3 + \ldots \quad (9)$$

where $\Gamma_{\alpha\beta} = 2\sin(\omega_{\alpha\beta}/2)$, $\omega_{\alpha\beta}$ being the angle formed by the sinks α and β with respect to the origin. Eqn (9) makes it very clear that the configuration of competitive reactive boundaries does influence the screening effect on the central sink. A clear signature of this is also that the corrections in eqn (9) alternate in sign. This behavior sheds considerable light on the many-body character of the rate constant, whose perturbative series is alternatively reduced by the diffusive interactions between the screening boundaries and the sink (shielding the ligand flux from it) and increased by the diffusive interactions among the screening particles (shielding the flux from each other). In contrast, the screening action of inert obstacles is largely dominated by the excluded-volume effect, and thus can only yield negative corrections at all orders.

Due to its perturbative nature, eqn (9) can be used to quantify the shielding action of specific 3D arrangements of sinks only for $N\varepsilon \propto N/d \ll 1$.[44] However, it still provides a powerful analytical tool to compare different geometries, as the perturbative rate is always proportional to the true rate (see ESI†). For example, eqn (9) could be used to design the special

configurations that minimize or maximize the screening effect on the central sink for the given values of N and d.

The average shielding action exerted by N equidistant sinks can be easily obtained analytically in the monopole approximation, *i.e.* by keeping only the $\ell = 0$ and $q = 0$ terms in eqn (6). The ensuing reduced system can be averaged over different configurations in the hypothesis of vanishing many-body spatial correlations, *i.e.* by integrating over the probability density $\mathscr{P}_N = \prod_{\alpha\neq\beta} (\sin\omega_{\alpha\beta})/4\pi$, with $2\arcsin(\sigma_1/d) \leq \omega_{\alpha\beta} \leq \pi$ (excluded-volume constraint between screening sinks). The result is (see ESI† for the details)

$$\left\langle \frac{k}{k_S} \right\rangle = \frac{1-\lambda\varepsilon[N-(N-1)(1-\lambda\varepsilon)]}{1-\lambda\varepsilon[N\varepsilon-(N-1)(1-\lambda\varepsilon)]} \qquad (10)$$

Fig. 3 shows that for $\lambda = 1$, eqn (10) provides an extremely good estimate of the configurational averages of the exact results at separations greater than a few diameters, highlighting the dramatic screening action of competitive reactive boundaries with respect to inert obstacles. Furthermore, a simple analysis of the rate fluctuations over the configuration ensembles at a fixed d allows one to gauge how sensitive competitive screening is to the specific 3D arrangement of the sinks. Remarkably, this analysis reveals stretches between the minimum and maximum rates for a given value of d as high as 40% of the average (see shaded bands in Fig. 3). More precisely, we remark that the variability associated with different geometries is greater (i) at short distances and (ii) for few screening particles.

Eqn (8)–(10) and the ensuing arguments are rather exemplary illustrations of the powerful analytical insight afforded by our general approach. The case of small screening sinks, $\lambda < 1$, provides a further demonstration of non-trivial effects that are captured by our analysis. It turns out that the function (10) displays a minimum for certain choices of the parameter N, λ. More precisely, a minimum exists at a fixed N for $\lambda \leq \lambda^*(N) \equiv (\sqrt{4N+1}-1)/(2N) < 1$, or, alternatively, at a fixed λ for $N \leq N^*(\lambda) \equiv (1-\lambda)/\lambda^2$. Fig. 4 provides a clear illustration of this subtle effect.

The flux into a large sink features a minimum for screening configurations of tiny absorbing particles close to its surface. This is the result of the competition between two effects. When the small particles lie very close to the surface of the large sink $\mathscr{S}_\sigma$, the latter behaves as an effective isolated sink of size $\sigma_{\text{eff}} < \sigma$, absorbing a flux $\Phi_{\text{eff}} = 4\pi D\sigma_{\text{eff}} \lesssim k_S$. Upon increasing the distance d, the total flux to the screening sinks will increase (their active surfaces get larger and they also get farther apart from each other). Now it is clear that the effect of this on the flux to $\mathscr{S}_\sigma$ will depend on the size of the screening particles. If σ_1 is small enough, σ_{eff} is not much smaller than σ, so that $\Phi_{d=\sigma+\sigma_1} \equiv \Phi_{\text{eff}}$ is not much smaller than $\Phi_\infty = k_S$. Under these conditions, the flux into the large sink starts decreasing, as the screening ensemble effectively steals more and more flux from it. However, upon increasing d past a critical distance, the small particles can no longer catch enough ligand flux, so that the flux to $\mathscr{S}_\sigma$ starts increasing, as it should, towards k_S.

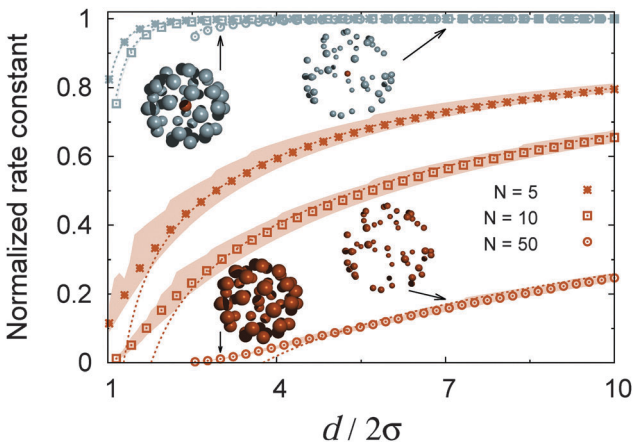

Fig. 3 Competitive screening greatly reduces the rate constant compared to inert obstacles, and is strongly modulated by the configuration. The total flux into a sink of radius σ surrounded by N spherical boundaries of the same size is arranged randomly at distance d (normalized to $k_S = 4\pi D\sigma$). Symbols denote the exact results (solution of eqn (6)), averaged over 100 independent configurations for each value of d. The shaded bands highlight the regions comprised between the minimum and maximum rates. For reflecting screening boundaries, these regions are as small as the truncation error. The light blue and orange lines are plots of eqn (8) and (10), respectively, with $\lambda = 1$. The arrows flag values of d corresponding to the two configurations shown ($N = 50$) with the screening spheres made all absorbing (bottom) and all reflecting.

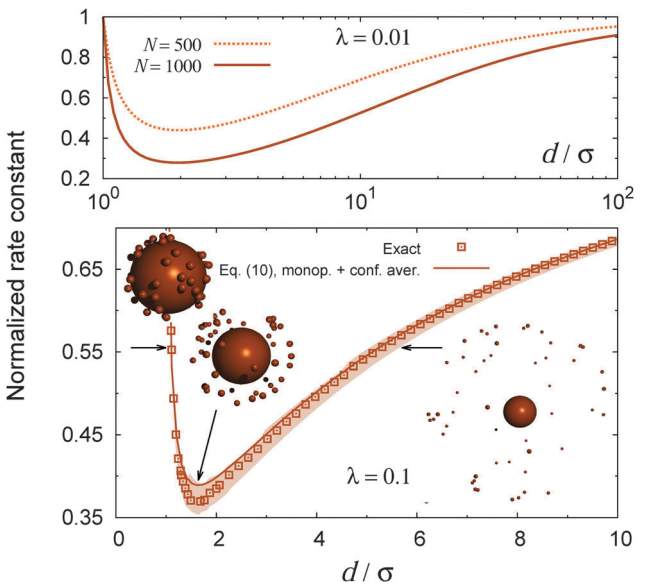

Fig. 4 Making the screening boundaries smaller makes the flux into the sink non-monotonic. Total flux into a sink of radius σ surrounded by $N = 50$ smaller sinks of radius $\sigma_1 = \sigma/10$ is arranged randomly at a distance d (normalized to $k_S = 4\pi D\sigma$). The left-most and right-most cartoons depict two configurations that screen exactly the same amount of flux, despite being at considerably different distances ($d/\sigma = 1.1$ and $d/\sigma = 8$). The configuration shown in the middle corresponds to the predicted minimum at $d/\sigma = 1 + \sqrt{1-\lambda[1+(N-1)\lambda]} \approx 1.64$. The solid line is a plot of formula (10). Each symbol is the average over 250 independent configurations, while the filled band comprises the region between the minimum and maximum rates. The top panel illustrates the case of screening by a large number of tiny particles, highlighting the sizeable non-monotonic effect. The curves are plots of eqn (10).

Summarizing, in this paper we have introduced a general theoretical framework to quantify how the geometry and distributed reactivity patterns of the environment modulate the rate constant of diffusion-influenced chemical reactions. Our method can be used to examine arbitrary reactive landscapes, made by assembling spherical boundaries of selected size at given locations in space and endowed with arbitrary surface reactivity. Moreover, our method can be extended to Laplace space,[45,46] so as to work out exactly the effect of the environment on time-dependent problems. This technique could be employed to shed further light on the intriguing sensitivity of time-dependent effects on initial conditions, which seems to constitute a rather generic feature of complex media.[22]

Finally, we stress that our method can be easily employed to derive approximate closed analytical formulas, which can be used to investigate naturally occurring reactive geometries and assist in the design of effective artificial nano-reactors for different technological applications.

Acknowledgements

The authors wish to thank P. De Los Rios and G. Foffi for insightful comments. F. P. and D. F. acknowledge joint funding from the French CNRS (PICS).

References

1 *Diffusion-limited reactions*, ed. S. A. Rice, Elsevier, Amsterdam, 1985, vol. 25.
2 A. Szabo, *J. Phys. Chem.*, 1989, **93**, 6929–6939.
3 G. Foffi, A. Pastore, F. Piazza and P. A. Temussi, *Phys. Biol.*, 2013, **10**, 040301.
4 J. Schöneberg and F. Noé, *PLoS One*, 2013, **8**, e74261.
5 K. Seki, M. Wojcik and M. Tachiya, *Phys. Rev. E: Stat., Nonlinear, Soft Matter Phys.*, 2012, **85**, 011131.
6 N. Dorsaz, C. De Michele, F. Piazza, P. De Los Rios and G. Foffi, *Phys. Rev. Lett.*, 2010, **105**, 120601.
7 J. D. Schmit, E. Kamber and J. Kondev, *Phys. Rev. Lett.*, 2009, **102**, 218302.
8 D. Ridgway, G. Broderick, A. Lopez-Campistrous, M. Ru'aini, P. Winter, M. Hamilton, P. Boulanger, A. Kovalenko and M. J. Ellison, *Biophys. J.*, 2008, **94**, 3748–3759.
9 D. ben Avraham and S. Havlin, *Diffusion and Reactions in Fractals and Disordered Systems*, Cambridge University Press, 2000.
10 P. P. Mitra, P. N. Sen, L. M. Schwartz and P. Le Doussal, *Phys. Rev. Lett.*, 1992, **68**, 3555–3558.
11 Y. Lu and M. Ballauff, *Prog. Polym. Sci.*, 2011, **36**, 767–792.
12 N. Welsch, A. Wittemann and M. Ballauff, *J. Phys. Chem. B*, 2009, **113**, 16039–16045.
13 K. T. Brady and J. E. Reiner, *J. Chem. Phys.*, 2015, **143**, 074904.
14 Y. Gao, Y. Chen, X. Ji, X. He, Q. Yin, Z. Zhang, J. Shi and Y. Li, *ACS Nano*, 2011, **5**, 9788–9798.
15 J. L. Vivero-Escoto, I. I. Slowing, B. G. Trewyn and V. S.-Y. Lin, *Small*, 2010, **6**, 1952–1967.
16 M. von Smoluchowski, *Phys. Z.*, 1916, **17**, 557–571.
17 O. Bénichou, C. Chevalier, J. Klafter, B. Meyer and R. Voituriez, *Nat. Chem.*, 2010, **2**, 472–477.
18 M. F. Shlesinger, G. M. Zaslavsky and J. Klafter, *Nature*, 1993, **363**, 31–37.
19 R. Kopelman, *Science*, 1988, **241**, 1620–1626.
20 R. J. Ellis, *Curr. Opin. Struct. Biol.*, 2001, **11**, 114–119.
21 H. X. Zhou, G. Rivas and A. P. Minton, *Annu. Rev. Biophys.*, 2008, **37**, 375–397.
22 O. Bénichou, C. Chevalier, J. Klafter, B. Meyer and R. Voituriez, *Nat. Chem.*, 2010, **2**, 472–477.
23 J. S. Kim and A. Yethiraj, *Biophys. J.*, 2009, **96**, 1333–1340.
24 J. A. Dix and A. Verkman, *Annu. Rev. Biophys.*, 2008, **37**, 247–263.
25 K. Luby-Phelps, *Int. Rev. Cytol.*, 2000, **192**, 189–221.
26 J. Kurzidim, D. Coslovich and G. Kahl, *J. Phys.: Condens. Matter*, 2011, **23**, 234122.
27 B. Nguyen and D. Grebenkov, *J. Stat. Phys.*, 2010, **141**, 532–554.
28 J. Kurzidim, D. Coslovich and G. Kahl, *Phys. Rev. Lett.*, 2009, **103**, 138303.
29 I. L. Novak, P. Kraikivski and B. M. Slepchenko, *Biophys. J.*, 2009, **97**, 758–767.
30 P. S. Burada, P. Hänggi, F. Marchesoni, G. Schmid and P. Talkner, *ChemPhysChem*, 2009, **10**, 45–54.
31 I. C. Kim and S. Torquato, *J. Chem. Phys.*, 1992, **96**, 1498–1503.
32 F. Piazza, G. Foffi and C. De Michele, *J. Phys.: Condens. Matter*, 2013, **25**, 245101.
33 M. von Smoluchowski, *Z. Phys. Chem.*, 1917, **92**, 129–168.
34 P. Debye, *Trans. Electrochem. Soc.*, 1942, **82**, 265.
35 F. C. Collins and G. E. Kimball, *J. Colloid Sci.*, 1949, **4**, 425–437.
36 M. Müller and N. Lebovka, *Advances in Polymer Science*, Springer, Berlin, Heidelberg, 2014, vol. 255, pp. 57–96.
37 G. Oshanin, M. Moreau and S. Burlatsky, *Adv. Colloid Interface Sci.*, 1994, **49**, 1–46.
38 S. D. Traytak, *Chem. Phys. Lett.*, 1992, **197**, 247–254.
39 S. D. Traytak, *Chemical Physics*, 1995, **193**, 351–366.
40 C. Eun, P. M. Kekenes-Huskey and J. A. McCammon, *J. Chem. Phys.*, 2013, **139**, 044117.
41 M. Galanti, D. Fanelli and F. Piazza, *Sci. Rep.*, 2016, **6**, 18976.
42 P. M. Morse and H. Feshbach, *Methods of theoretical physics*, McGraw-Hill Science/Engineering/Math, 1953, vol. 2, pp. 409–415.
43 S. D. Traytak, *Journal of Composite Mechanics and Design*, 2003, **9**, 495–521.
44 S. D. Traytak, *Phys. A*, 2006, **362**, 240–248.
45 E. Gordeliy, S. L. Crouch and S. G. Mogilevskaya, *International Journal for Numerical Methods in Engineering*, 2009, **77**, 751–775.
46 S. D. Traytak, *Chem. Phys. Lett.*, 2008, **453**, 212–216.